High-Temperature Superconducting Nonlinear Transmission Lines

Gordon M. Coutts, Raafat R. Mansour, *Senior Member, IEEE*, and S. K. Chaudhuri, *Senior Member, IEEE*

***Abstract*—This paper introduces novel potential device applications based on the nonlinear phase shifting properties of high-temperature superconductor (HTS) transmission lines. It demonstrates how the nonlinear characteristics of HTS materials can be used to build devices that improve the risetime of pulses as well as exhibit power-dependent phase shifting properties. The nonlinear transmission-line circuit layouts consist of a linear transmission-line periodically loaded with HTS stubs operating in the nonlinear region. Theoretical results are presented using a lumped-element SPICE model to verify the pulse-shaping concept presented in this paper. The power-dependent phase shifting properties are demonstrated with the measurements of two prototype circuits.**

***Index Terms*—High-temperature superconductor (HTS), nonlinear transmission line (NLTL), , pulse sharpening, risetime improvement, power-dependent phase shifter, shockline.**

I. Introduction

THE need for generating pulses with faster risetime values increases as frequency levels used in microwave and millimeter-wave applications increase. Such high-frequency applications require the availability of circuits that are capable of generating pulses having 0.1–5 ps risetimes. The relatively fast pulse risetime values impose limits on the sampling and detection of high-frequency signals. A nonlinear transmission line (NLTL) can be used to decrease the risetime of a propagating pulse by forming a shock wave [1]–[3]. Shock waves arise in nonlinear media when the propagation velocity has an amplitude dependence that causes the leading edge of a pulse to get steeper. An analysis of shock-wave generation in a transmission line loaded with Josephson junctions is given in [4].

Conventional NLTLs have been realized using linear transmission lines that are periodically loaded with varactor diodes [1]. A varactor diode exhibits a voltage-dependent capacitance when reverse biased. This voltage dependence can be used to realize an NLTL circuit capable of decreasing the rise time of a pulse. Recent work has demonstrated effective NLTL applications in measurement instruments that require sampling down converters. Such applications include phase locked synthesizers, frequency counters, network analyzers, and oscilloscopes [2]. With the use of a monolithic microwave integrated circuit NLTL, researchers at Hewlett-Packard have constructed a commercially viable sampler with a 55-GHz useable bandwidth as well as greater conversion efficiency over conventional samplers [2].

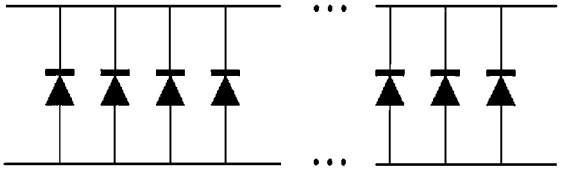

Fig. 1. A conventional nonlinear transmission line.

The performance of a nonlinear transmission line is limited by several factors, including the diode cutoff frequency. Other disadvantages include high values of insertion loss as well as significant power dissipation due to the required biasing of the numerous diodes that form the NLTL.

In this paper, we demonstrate that one can build an NLTL by periodically loading a transmission line with high-termperature superconductor (HTS) stubs that exhibit nonlinear performance. The stubs are chosen to be thin enough to allow operation within the nonlinear region. The HTS NLTL pulse-shaping effects are demonstrated using a SPICE model combined with an HTS nonlinear analysis that is validated with published data. First, a conventional varactor diode NLTL is simulated using SPICE. The varactor diodes are then replaced with a SPICE model of the nonlinear HTS stubs to form the lumped-element HTS NLTL model.

In addition to shaping pulses, the HTS NLTL circuits exhibit power-dependent phase-shifting properties that can be controlled through the choice of circuit geometry. We also present in this paper experimental and theoretical results for the power-dependent phase-shifting performance of two different HTS NLTL prototype circuits.

II. Conventional NonLinear Transmission Lines

Fig. 1 illustrates the conventional NLTL. It consists of a linear transmission line periodically loaded with varactor diodes that exhibit a voltage-dependent capacitance when reverse biased.

As shown in Fig. 2, the equivalent circuit model of a NLTL segment is a lumped-element linear transmission-line model augmented with a nonlinear capacitor. The linear transmission line consists of a series inductor $L_{\rm TL}$ and a shunt capacitor $C_{\rm TL}$. The nonlinear capacitor $C_{\rm NL}$ is dependent on the voltage amplitude. A series of cascaded lumped model segments, as shown in Fig. 3, forms a simplified model of a NLTL.

Manuscript received February 29, 2000; revised August 23, 2000.

G. M. Coutts was with the Department of Electrical and Computer Engineering, University of Waterloo, Waterloo, ON, Canada. He is now with Agilent Technologies, Rohnert Park, CA, 94928 USA.

R. R. Mansour was with the Corporate Research and development department, COM DEV Ltd., Cambridge, Ont., Canada. He is now with the Department of Electrical and Computer Engineering, University of Waterloo, Waterloo, ON, Canada.

S. K. Chaudhuri is with the Department of Electrical and Computer Engineering, University of Waterloo, Waterloo, ON, Canada.

Publisher Item Identifier S 0018-9480(00)10782-3.

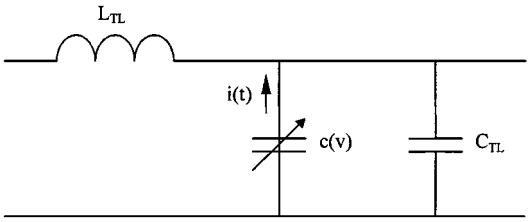

Fig. 2. Lumped-element nonlinear transmission-line segment model.

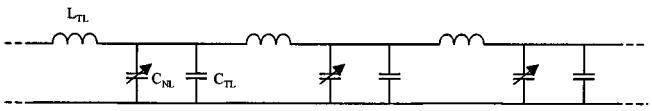

Fig. 3. Lumped-element nonlinear transmission-line model.

The total NLTL segment capacitance is the sum of the linear and nonlinear capacitor values, given by

$$C_T(V) = C_{\rm TL} + C_{\rm NL}(V). \tag{1}$$

The propagation delay along each transmission-line segment is given by

$$T(V) = \sqrt{L_{\rm TL} C_T(V)}. \tag{2}$$

The voltage-dependent capacitors that periodically load the transmission line can lead to shock-wave formation with electrical pulses. As can be seen in (2), the time delay along the transmission line becomes greater with increasing capacitance. The total delay along the transmission line is the delay along each segment times the number of segments. If the capacitance increases with voltage, the time delay of the higher voltage portion of a signal increases. For a ramped pulse, an increased delay for higher voltages results in a steeper edge, as shown in Fig. 4.

A lumped-element equivalent circuit model of a transmission line periodically loaded with varactor diodes can be simulated using SPICE. The analysis uses the varactor NLTL modeling technique outlined in [1]. The uniformly doped Schottky diode has a capacitance given by

$$C_d(V) = \frac{C_{j0}}{\sqrt{1 - \frac{V}{\phi}}} \tag{3}$$

where ϕ is the barrier potential, which is approximately 0.8 V for a uniformly doped diode. The nonlinear diode capacitance can be represented in SPICE using a voltage-dependent current source and a fixed capacitor. The SPICE model can be derived by rearranging the diode model equations, expressing the capacitor current $i(t)$ in terms of the capacitor voltage (see Fig. 2). Using (3), the current emerging from the nonlinear capacitor, expressed in terms of the capacitance and voltage, is approximated by

$$i(t) \approx c(V)\frac{dV}{dt} = \frac{C_{j0}}{\sqrt{1 - \frac{V}{\phi}}}\frac{dV}{dt}. \tag{4}$$

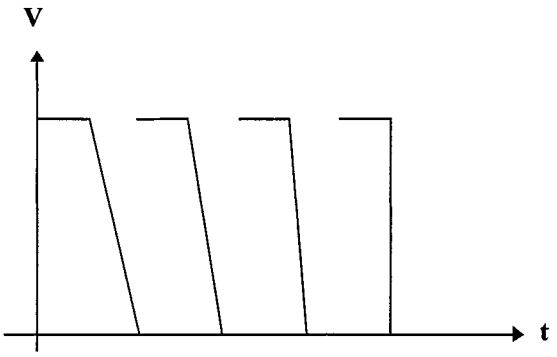

Fig. 4. Leading-edge steepening due to the nonlinear capacitance.

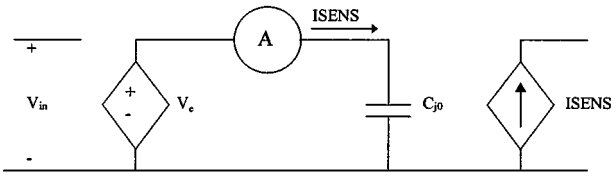

Fig. 5. Nonlinear capacitor SPICE model.

Equation (4) can be expressed in terms of the capacitor C_{j0} with an effective applied voltage level V_e

$$i(t) = C_{j0}\frac{dV_e}{dt}. \tag{5}$$

The effective applied voltage level is

$$V_e = -2\phi\sqrt{1 - \frac{V}{\phi}}. \tag{6}$$

The SPICE model applies the voltage signal V_e to the capacitor C_{j0}. The V_e signal can be implemented using a voltage-dependent voltage source with a dependency given by (6) with V equal to the voltage across the nonlinear capacitor. Fig. 5 shows the SPICE model implementation of the nonlinear capacitor.

A current-dependent current source at the output samples the current flowing through the capacitor C_{j0} and outputs that exact current value. The SPICE model of the entire NLTL is a series of the cascaded transmission-line segments shown in Fig. 5.

Fig. 6 shows the SPICE simulation results of a 100-element NLTL periodically loaded with varactor diodes having $C_{j0} =$ 0.1 pF and $\phi = 0.8$. The center transmission line has a 50-Ω characteristic impedance. The falltime improvement trend using this type of diode is consistent with results achieved in [1]. For a 10-V input pulse, the 10–90% falltime of the input pulse is 80 ps, and the output falltime is 24.6 ps.

III. Lumped-Element Modeling of HTS NLTL Circuits

The varactor diode exhibits a voltage-dependent capacitance that can shape a pulse as it propagates down the transmission line. A similar effect may be achieved using narrow stubs of HTS material that are designed to operate in the nonlinear region.

The stubs are chosen such that the nonlinear effect due to the HTS material results in a variation in the equivalent capacitance of the open-circuit stubs. A nonlinear transmission line can thus

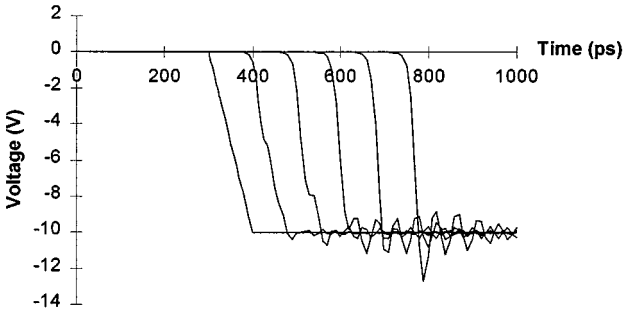

Fig. 6. Falltime improvement: input pulse, pulse after 20, 40, 60, 80, and 100 diodes.

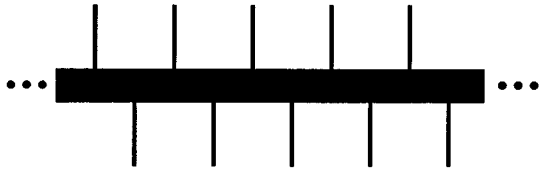

Fig. 7. HTS NLTL layout.

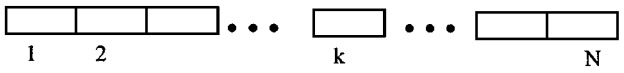

Fig. 8. Division of the HTS planar transmission line into N subsections.

be fabricated using an HTS microstrip structure consisting of a wide center transmission line periodically loaded with narrow open-circuited stubs, as shown in Fig. 7. The center transmission line is assumed to be wide such that it operates in the linear region. The stubs, which are narrow relative to the center line, are designed to operate in the nonlinear region.

The nonlinear effects on the HTS stubs are modeled using the method discussed in [5]. Consider the HTS transmission line shown in Fig. 8. The line is divided into N cascaded subsections each of length Δx. The propagation and attenuation constants vary with the instantaneous level of voltage along the transmission line. We assume that the phase shift and attenuation along a single subsection are constant values $\beta\Delta x$ and $\alpha\Delta x$ for a given instant in time.

In [6], a nonlinear full-wave solution based on Ginzburg–Landau (GL) theory is developed using the finite-difference time-domain technique. The theoretical results given in [6] show that the propagation constant β and attenuation constant α of HTS transmission lines vary linearly with applied power at the levels that are typically used for third-order intercept (TOI) measurements. The propagation and attenuation constants along each subsection can thus be approximated by

$$\beta = \beta_0 \left(1 + \frac{a_1}{w^2}|V|^2\right) \tag{7}$$

$$\alpha = \alpha_0 \left(1 + \frac{a_2}{w^2}|V|^2\right) \tag{8}$$

where β_0 and α_0 are, respectively, the low power propagation and attenuation constants of the HTS transmission line. The value w is the transmission-line width in micrometers. The constants a_1 and a_2 are functions of the material characteristics and are to be evaluated by fitting the TOI curves generated from the proposed model to measured data.

For the kth subsection at a given instant in time, the voltage can be written as

$$V_k = V_{k-1}\cos(\omega t - \beta_k \Delta x)e^{-\alpha_k \Delta x} \tag{9}$$

where β_k and α_k are given by

$$\beta_k = \beta_0 \left[1 + \frac{a_1}{w^2}\left|V_{k-1}\cos(\omega t - \beta_{k-1}\Delta x)e^{-\alpha_{k-1}\Delta x}\right|^2\right] \tag{10}$$

$$\alpha_k = \alpha_0 \left[1 + \frac{a_2}{w^2}\left|V_{k-1}\cos(\omega t - \beta_{k-1}\Delta x)e^{-\alpha_{k-1}\Delta x}\right|^2\right]. \tag{11}$$

The signal components at the fundamental frequency and harmonics are calculated at the output of each subsection by taking a complex fast Fourier transform of the time-domain waveform of (9). This signal is then applied to the next nonlinear subsection, leading to the generation of a new set of harmonics. The level of the harmonics then builds progressively through each cascaded subsection until reaching the end of the transmission line. Fig. 9 illustrates the concept of the nonlinear model.

The nonlinear model was validated using data published by Wilker *et al.* [8]. The measured data are for single-tone TOI of a series of 50-Ω $Tl_2Ba_2CaCu_2O_8$ (TBCCO) coplanar transmission lines of varying widths and lengths. The substrate used is $LaAlO_3$ with a value $\varepsilon_r = 24$ and $\tan\delta = 10^{-5}$. A stimulus frequency of 1.5 GHz was used in simulating the transmission line. The input power was stepped from 0 to 40 dBm. The constants a_1 and a_2 were set to the values corresponding to the temperature, and the length of the line was varied in accordance with the measured results. The constants a_1 and a_2 are only valid for a single temperature since the nonlinear effects increase as the temperature approaches the critical value. The optimized values for these constants at 90 and 100 K are given in Table I. As expected, the nonlinear effects are more pronounced at 100 K, as indicated by the higher constant values.

According to Megahed *et al.* [6], the nonlinear effect of the attenuation constant is greater than for the phase velocity (and thus β). This difference arises since the ohmic attenuation effect is greater than the change in stored kinetic energy that causes the shift in phase velocity [6]. The optimized constants are consistent with the results of Megahed *et al.* As seen in Table I, the attenuation model constant a_2 is higher than that of the phase model constant a_1.

Table II illustrates the third-order intercept values for different line widths. The calculated values of the TOI points correlated very well with the published results from Wilker *et al.* [8]. As shown in Tables II and III, the model accurately predicts the variations of the third-order intercept with respect to both line width and length. The results achieved are consistent with expectations since the current density is lower for a wider line. The current density is thus farther from the critical level and the nonlinear effect decreases. Table III indicates that an increase in line length yields a lower third-order intercept point. This was also expected since the signal propagates along a greater distance through the HTS line, augmenting the nonlinear effect.

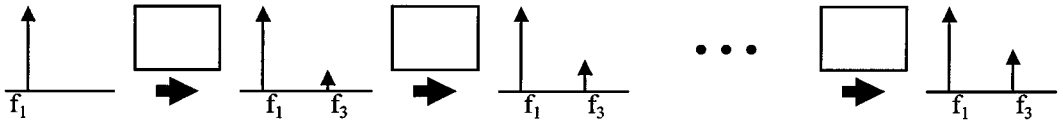

Fig. 9. The third harmonic level increases as the signal propagates through each segment of the HTS planar transmission line.

TABLE I
OPTIMIZED VALUES OF THE NONLINEAR PROPAGATION MODEL CONSTANTS a_1 AND a_2

T(K)	Optimized a_1	Optimized a_2
90	0.0148	0.7
100	0.58	12.85

TABLE II
COMPARISON OF MEASURED [8] VERSUS. CALCULATED TOI (dB) FOR VARYING LINE WIDTHS

T (K)	Width (μm)	Measured TOI (dB)	Calculated TOI (dB)	% Deviation from Measured Mean
90	56	71.2±0.9	70.3	1.3%
90	28	64.5±0.6	64.1	0.62%
90	7	51.3±0.7	52.0	1.4%
100	56	55.4±0.3	54.4	1.8%
100	28	48.5±0.4	48.4	0.21%
100	7	37.3±0.4	37.4	0.27%

TABLE III
COMPARISON OF MEASURED [8] VERSUS. CALCULATED TOI (dB) FOR VARYING LINE LENGTHS

T (K)	Length (mm)	Measured TOI (dB)	Calculated TOI (dB)	% Deviation from Measured Mean
90	14	64.5±0.6	64.1	0.62%
90	5	68.6±1.1	69.0	0.58%
90	1	75.0±?	78.1	4.0
100	14	48.5±0.4	48.4	0.21%
100	5	52.8±0.9	52.9	0.19%
100	1	60.4±2.4	59.9	0.83%

The data point for a 1-mm line at 90 K has an unknown measurement tolerance level [8]. The calculated value differed from the measured mean by 4%, which may be the result of greater measurement error. The other values corresponded well to the measured results, differing between 0.19% and 1.8% from the measured mean TOI level.

The validated nonlinear HTS model is used to characterize the stubs in the proposed NLTL topology of Fig. 7. The SPICE model developed in Section II yielded results consistent with [1] for a transmission line periodically loaded with diodes. The next step is to modify the voltage-dependent capacitor model such that it characterizes the nonlinear properties of the HTS materials.

The first step in modeling the HTS nonlinear transmission line is to develop a lumped voltage-dependent capacitor model of the open-circuited stub, based on the above HTS model. This provides an initial approximation of the HTS NLTL propagation characteristics.

The voltage-dependent capacitance arises from the change in the electrical length of an open-circuited HTS stub as the power level increases. The capacitance of the stub is calculated using (7), where $\beta_0 = \omega\sqrt{\mu\varepsilon}$. If the stub length l is small relative to the wavelength $(\tan\beta l \approx \beta l)$, the voltage dependent capacitance C can be approximated as

$$c(V) \approx \frac{\sqrt{\mu\varepsilon}\left(1+\frac{a_1}{w^2}|V|^2\right)l}{z_0} \tag{12}$$

where Z_0 is the characteristic impedance of the transmission-line stub. In view of (12), it can be seen that the capacitance value increases as the voltage level rises. As a result, the nonlinear HTS stubs will contribute to a decrease in the rise time of a pulse as it propagates down the periodic transmission line. It should be mentioned that the nonlinear capacitor model given in (12) is only valid up to the frequency range where the stub length l is still considered smaller than the wavelength.

The nonlinear capacitor model can be incorporated into a lumped-element SPICE model representation of the NLTL using the technique outlined for the varactor NLTL. In view of the analysis given in Section II, the SPICE model V_e can be written as

$$V_e = V + \frac{a_1}{3w^2}|V|^3. \tag{13}$$

The lumped inductor and capacitor models used to represent a transmission-line segment are calculated in terms of the distributed transmission-line parameters β and Z_0. The electromagnetic simulator Sonnet-EM was used to obtain the effective dielectric constant and characteristic impedance of the center transmission line as well as the stub line.

Fig. 10 shows the falltime improvement for a 20-V pulse along an HTS NLTL with a 50-Ω center line and stubs of length 50 mil and width 1 mil. The stub spacing is 10 mil. The 10–90% falltime of the input pulse is 80 ps, and the output falltime is 21.3 ps.

IV. POWER-DEPENDENT PHASE SHIFTER APPLICATION

In addition to sharpening pulses, the HTS NLTL circuits with topologies similar to that of Fig. 7 exhibit useful power-dependent phase-shifting properties. Such properties have been demonstrated with two HTS NLTL prototype circuits.

Each NLTL is constructed using a TBCCO film on a 20-mil-thick $LaAlO_3$ substrate. Fig. 11 shows the topology of the periodically loaded HTS microstrip NLTL.

Fig. 12 illustrates the layout of the two prototype circuits, while Table IV lists the parameters of the two prototype NLTL circuits TL1 and TL2.

The measurement technique used to observe the power-dependent phase-shifting properties of the prototype circuits uses

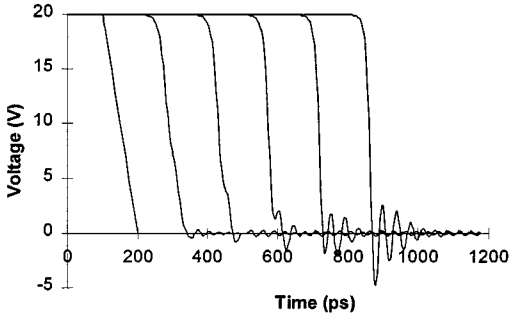

Fig. 10. Falltime improvement in HTS NLTL: input pulse, pulse after 20, 40, 60, 80, and 100 stubs.

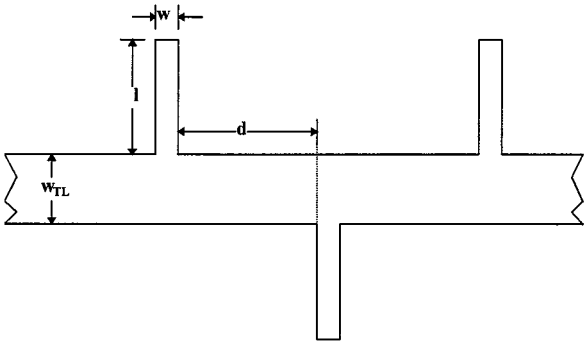

Fig. 11. Periodically loaded HTS microstrip NLTL.

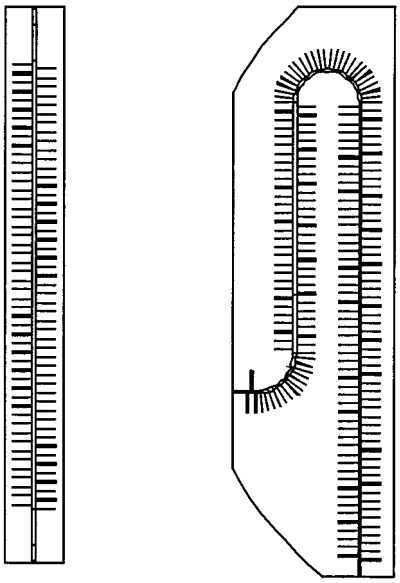

Fig. 12. NLTL prototype layout. TL1: left. TL2: right.

a continuous-wave signal generator and sampling oscilloscope to directly measure the attenuation and phase. The test set is shown in Fig. 13.

Figs. 14 and 15 show the results of the NLTL attenuation and phase measurements, respectively. As can be seen in Fig. 15, there is a small increase in the relative phase below the critical level. The measured phase then jumps sharply at the critical level. The nonlinear transmission line model can be used to predict the phase shifter performance below the critical level. The phase jump at the critical temperature requires a more detailed investigation of the HTS NLTL performance.

TABLE IV
PROTOTYPE NLTL PHYSICAL PARAMETERS

Parameter	TL1	TL2
N	100	209
Stub Impedance	70.8 Ω	70.8 Ω
L	50 mil	50 mil
W	1 mil	1 mil
D	10 mil	10 mil
w_{TL}	6.9 mil	6.9 mil
Centre Line Impedance	50 Ω	50 Ω

The center transmission line is 6.9 times wider than the open-circuited stubs. As a result, the stub current density is considerably higher than for the center line. The stubs will thus become nonsuperconductive before the center line reaches its critical level. This is a likely explanation of the sudden increase in the NLTL phase. To illustrate this theory, a set of Sonnet-EM simulations was carried out at 4-GHz using a straight, periodically loaded transmission line (see Fig. 16).

The S-parameters were simulated while increasing the metallization resistivity in increments of 0.1 Ω/square, representing an increase in the HTS surface resistance with increasing power. The next step was to remove stubs from the circuit, mimicking the effect of stubs becoming normally conducting.

As seen in Fig. 17, the S_{21} phase increases slightly with increasing resistivity and a constant number of stubs. The phase then increases in large increments as stubs are removed. The observed TL1 phase characteristics can thus be explained by a large number of stubs suddenly becoming nonsuperconductive at a given power level. Further work is required to incorporate the effect of stubs reaching the critical level into the HTS NLTL model.

Figs. 18 and 19 show the measured attenuation and phase of the TL2 prototype. The TL2 circuit exhibits an unusual phase response as the power level increases, as can be seen in Fig. 19. The electrical length of the circuit actually decreases up to a certain power level, and then the total phase shift along the line begins to increase. The sudden increase in the electrical length is accompanied by a sudden increase in attenuation.

As for the TL1 case, the phase shift properties can be explained using examples simulated with Sonnet-EM. Consider the lossless, curved periodically loaded structure of Fig. 20(a). A series of simulations were carried out at 4 GHz while increasing the resistivity in increments of 0.1 Ω/square to mimic the nonlinear increase in attenuation of the HTS material with increasing power. As seen in Fig. 21, the S_{21} phase actually decreases by 7.7° when the resistivity changes from 0 to 0.4 Ω/square.

As the input power rises, an increasing number of stubs will become nonsuperconductive before the center line reaches its critical level. This effect was simulated by progressively removing stubs from the circuit models. As can be seen in Fig. 20(b)–(d), circuits were simulated with four, eight, and 12 missing stubs, respectively (while continuing to increase the

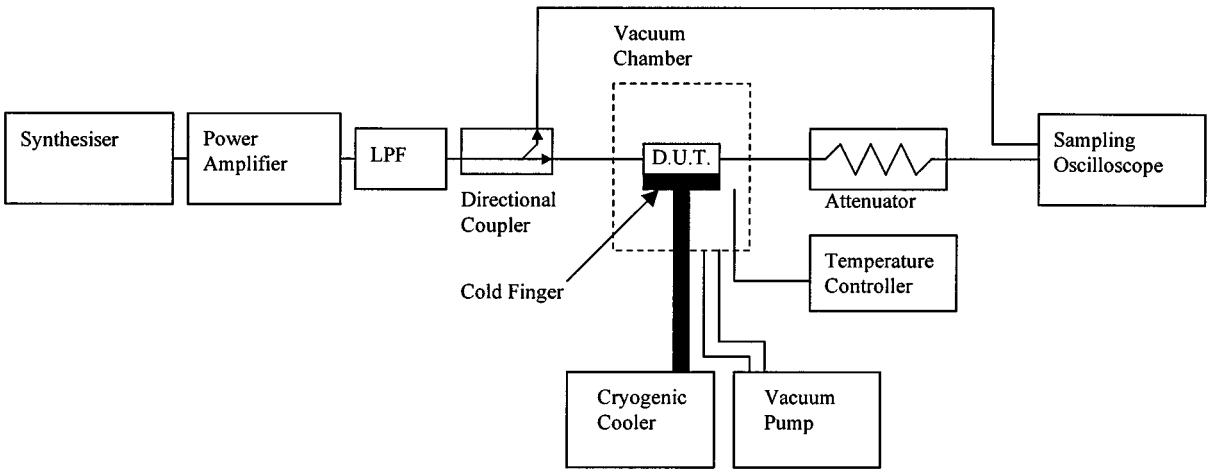

Fig. 13. High-power test set.

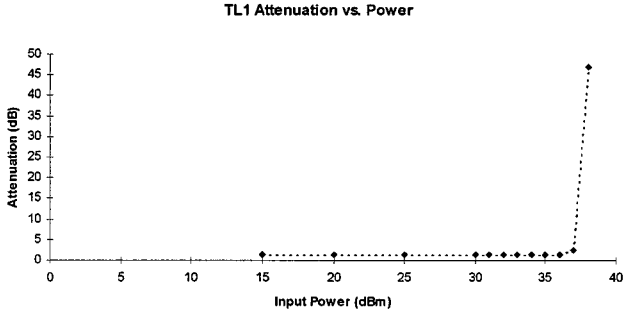

Fig. 14. TL1 attenuation measurement at 3.7 GHz.

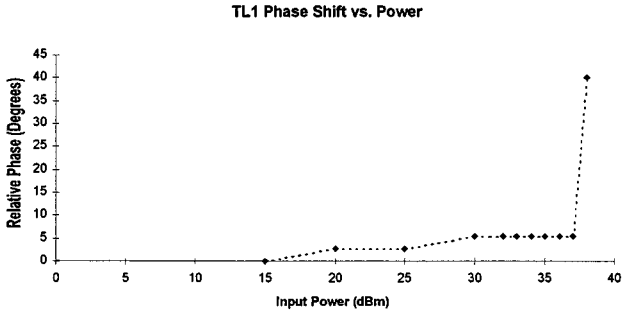

Fig. 15. TL1 phase measurement at 3.7 GHz.

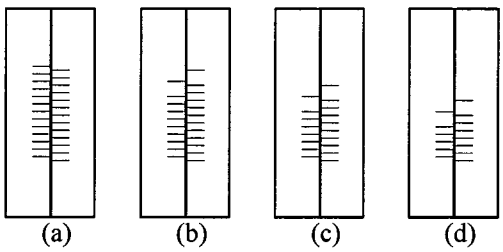

Fig. 16. (a) Straight line test circuit with (b) four, (c) eight, and (d) 12 stubs missing to simulate the effect of losses and removing stubs.

resistivity by 0.1 Ω/square for each successive simulation). Due to the attenuation along the HTS line, the power level is higher

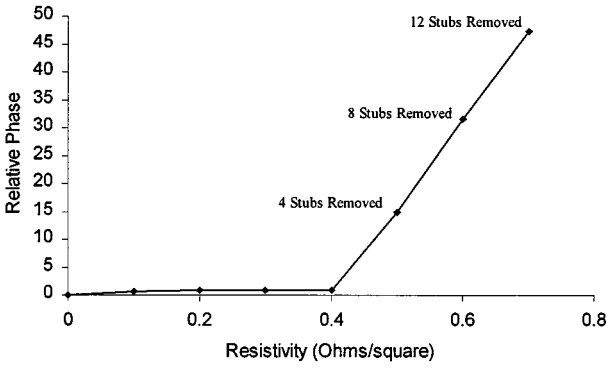

Fig. 17. Simulated relative S_{21} phase (4 GHz) of straight line test circuits.

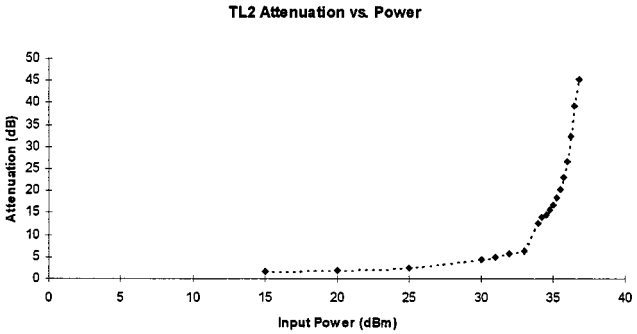

Fig. 18. TL2 amplitude measurement at 3.7 GHz.

toward the input side of the HTS circuits. The critical current levels of the stubs vary due to manufacturing tolerances. As it is difficult to predict the exact order in which stubs will become nonsuperconductive, the stubs were removed randomly, closer to the input side of the circuit (see Fig. 20).

As can be seen in Fig. 21, the S_{21} phase begins to increase dramatically with the removal of stubs. As shown using Sonnet-EM, the phase continues to increase, as more stubs become nonsuperconductive. The phase response trend of the curved test circuit follows the measured TL2 phase response of Fig. 19.

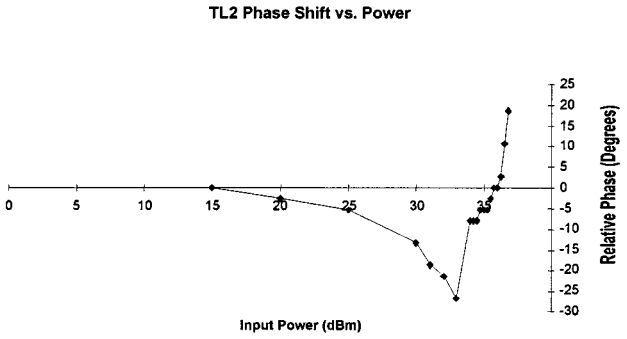

Fig. 19. TL2 relative phase measurement at 3.7 GHz.

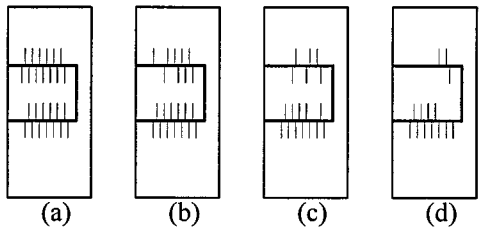

Fig. 20. (a) Curved line test circuit with (b) four, (c) eight, and (d) 12 stubs missing to simulate the effect of losses and removing stubs.

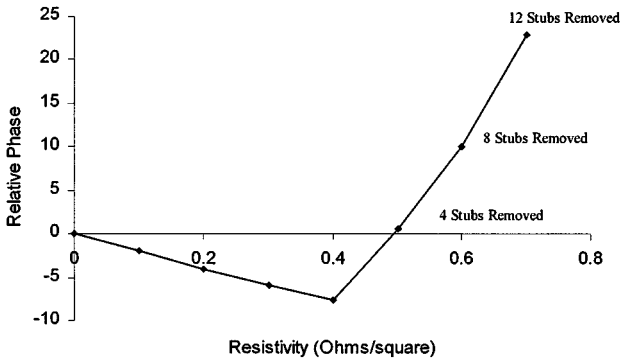

Fig. 21. Simulated relative S_{21} phase (4 GHz) of curved line test circuits.

As observed from the TL1 and TL2 measurements, given in Figs. 15 and 19, for values of input power below the levels that cause stubs to become nonsuperconductive, the phase increases for the straight line and decreases for the curved line. The phase decrease is likely due to the coupling of forward and backward propagating signals in the curved section of TL2. As the power increases, the attenuation increases, reducing the effect of coupling, causing a decrease in electrical length. Further work is required to include the coupling effects, as well as the progressive loss of superconducting stubs, in the HTS NLTL model for the TL2 geometry.

V. Concluding Remarks

This paper has demonstrated that the nonlinear characteristics of HTS materials can be used to realize NLTLs. A transmission line periodically loaded with thin HTS lines, which operate in the nonlinear region, has been theoretically shown to exhibit pulse-sharpening effects. The falltime improvements for the proposed circuit are in the range of 10–50 ps. The available test equipment was capable of generating a minimum risetime/falltime value of 40 ns. As a result, any falltime improvements due to the HTS NLTL circuit were a very small percentage of the input fall time. Such subtle improvements are beyond the detection limit of the equipment currently available to us. Future measurements are planned using a source capable of generating input risetime in the 100-ps range and a sampling oscilloscope with a small time scale limit.

Two HTS NLTL prototype circuits were shown to exhibit power-dependent phase-shifting properties. This effect was augmented by the tendency of the small stubs to become nonsuperconductive as the applied power increases, while the relatively wide center conductor remains superconductive. The phase characteristics may vary greatly depending on the HTS NLTL geometry.

References

[1] M. J. W. Rodwell, S. T. Allen, R. Y. Yu, M. G. Case, U. Bhattacharya, M. Reddy, E. Carman, M. Kamegawa, Y. Konishi, J. Pusl, and R. Pullela, "Active and nonlinear wave propagation devices in ultrafast electronics and optoelectronics," *Proc. IEEE*, vol. 82, no. 7, July 1994.

[2] W. C. Whiteley, W. E. Kunz, and W. J. Anklam, "50 GHz sampler hybrid utilizing a small shockline and an internal SRD," in *Proc. 1991 IEEE MTT-S Int. Microwave Symp.*, pp. 895–898.

[3] D. Jäger, "Characteristics of travelling waves along the nonlinear transmission lines for monolithic integrated circuits: A review," *Int. J. Electron.*, vol. 58, no. 4, pp. 649–669, 1995.

[4] G. Chen and M. R. Beasly, "Shock-wave generation and pulse sharpening on a series array Josephson junction transmission line," *IEEE Trans. Appl. Superconduct.*, vol. 1, pp. 140–144, Sept. 1991.

[5] G. M. Coutts, R. R. Mansour, and S. K. Chaudhuri, "A novel approach to modeling the nonlinear propagation characteristics of HTS planar transmission lines," presented at the IEEE MTT-S Int. Microwave Symp., 1998.

[6] M. A. Megahed and S. M. El-Ghazaly, "Nonlinear analysis of microwave superconductor devices using full-wave electromagnetic model," *IEEE Trans. Microwave Theory Tech.*, vol. 43, pp. 2590–2598, Nov. 1995.

[7] O. G. Vendik, I. B. Vendik, and T. B. Samoilova, "Nonlinearity of superconducting transmission line and microstrip resonator," *IEEE Trans. Microwave Theory Tech.*, vol. 45, pp. 173–178, Feb. 1997.

[8] C. Wilker, Z.-Y. Shen, P. Pang, W. L. Holstein, and D. W. Face, "Nonlinear effects in high temperature superconductors: 3rd order intercept from harmonic generation," *IEEE Trans. Appl. Superconduct.*, vol. 5, pp. 1665–1670, June 1995.

[9] C.-W. Lam, D. M. Sheen, S. M. Ali, and D. E. Oates, "Modeling the nonlinearity of superconducting strip transmission lines," *IEEE Trans. Appl. Superconduct.*, vol. 2, pp. 58–65, June 1992.

[10] J. H. Oates, R. T. Shin, D. E. Oates, M. J. Tsuk, and P. P. Nguyen, "A nonlinear transmission line model for superconducting stripline resonators," *IEEE Trans. Appl. Superconduct.*, vol. 3, pp. 17–22, Mar. 1993.

[11] *Handbook of Microwave Integrated Circuits*, Artech House, MA, 1987.

Gordon M. Coutts was born in Ottawa, Ont., Canada. He received the B.A.Sc. degree in electrical engineering (co-op) and the M.A.Sc. degree from the University of Waterloo, Waterloo, ON, Canada, in 1998 and 1999, respectively.

His research investigated the nonlinear propagation characteristics of high-temperature superconducting planar transmission lines and applications. His master's research was conducted with the support of COM DEV Ltd., Cambridge, ON, Canada, the University of Waterloo, and the Natural Sciences and Engineering Research Council of Canada. In December 1999, he joined Agilent Technologies in Rohnert Park, CA.

Raafat R. Mansour (S'84–M'86–SM'90) was born in Cairo, Egypt, on March 31, 1955. He received the B.Sc. (with honors) and M.Sc. degrees from Ain Shams University, Cairo, Egypt, in 1977 and 1981, respectively, and the Ph.D. degree from University of Waterloo, Waterloo, ON. Canada in 1986, all in electrical engineering.

In 1991, he was a Research Fellow at the laboratoire d'Electromagnetisme, Institut National Polytechnique, Grenoble, France. From 1983 to 1986, he was a Research and Teaching Assistant with the Department of Electrical Engineering, University of Waterloo. He then joined COM DEV Ltd. Cambridge, ON, Canada, where he held several technical and management positions in the Corporate Research and Development Department, and in 1998, was promoted to Staff Scientist. In January 2000, he joined the Electrical and Computer Engineering Department, University of Waterloo, where he is currently a Professor. He has authored or co-authored numerous publications in the area of electromagnetic modeling and HTS and holds several patents related to microwave filter design for satellite applications. His current research interests include superconductive technology, microelectromechanical (MEMS) technology, and computer-aided design (CAD) of RF circuits for wireless and satellite applications.

S. K. Chaudhuri (M'79–SM'85) was born in Calcutta, India, on August 25, 1949. He received the B.E. degree (with honors) in electronics engineering from the Birla Institute of Technology and Science, Pilani, India, and the M.Tech. degree in electrical communication engineering from the Indian Institute of Technology, Delhi, India, in 1970 and 1972, respectively, and the M.A.Sc. degree in microwave engineering and the Ph.D. degree in electromagnetic theory from the University of Manitoba, Winnipeg, Man., Canada, in 1973 and 1977, respectively.

In 1977, he joined the University of Waterloo, where he is currently a Professor in the Electrical and Computer Engineering Department and the Dean of the faculty of engineering. He held a Visiting Associate Professor's position in the Electrical Engineering and Computer Science Department, University of Illinois at Urbana-Champaign, in 1981 and 1984. He held a Visiting Professorship at the National University of Singapore from 1990 to 1991, and an Erskine Fellowship at the University of Canterbury, Canterbury, New Zealand, in 1998. He has been involved in contact research and consulting work with several Canadian and U.S. industries and government research organizations. His current research interests are in guided-wave/electrooptic structures, planar microwave structures, dielectric resonators, optical and electroluminescent imaging, and the fiber-base broad-band network.

Dr. Chaudhuri is a member of URSI Communication B and Sigma Xi.